Ponderomotive acceleration of hot electrons in tenuous plasmas

V. I. Geyko and G. M. Fraiman
Institute of Applied Physics, RAS, 46 Ulyanov Street, Nizhny Novgorod 603950, Russia

I. Y. Dodin and N. J. Fisch
Department of Astrophysical Sciences, Princeton University, Princeton, New Jersey 08544, USA
(Received 9 February 2009; published 15 September 2009)

The oscillation-center Hamiltonian is derived for a relativistic electron injected with an arbitrary momentum in a linearly polarized laser pulse propagating in tenuous plasma, assuming that the pulse length is smaller than the plasma wavelength. For hot electrons generated by collisions with ions under an intense laser drive, multiple regimes of ponderomotive acceleration are identified, and the laser dispersion is shown to affect the process at plasma densities down to 10^{17} cm^{-3}. We consider the regime when the cold plasma is not accelerated, requiring $a/\gamma_g \ll 1$, where a is the laser parameter, proportional to the field amplitude, and γ_g is the group-velocity Lorentz factor. In this case, the Lorentz factor γ of hot electrons does not exceed $\Gamma \equiv a\gamma_g$ after acceleration, assuming its initial value also satisfies $\gamma_0 \lesssim \Gamma$. Yet $\gamma \sim \Gamma$ is attained within a wide range of initial conditions; hence, a cutoff in the hot-electron distribution is predicted.

DOI: 10.1103/PhysRevE.80.036404 PACS number(s): 52.38.Kd, 52.20.Fs, 45.20.Jj, 41.75.Ht

I. INTRODUCTION

Recent advances in laser technology have yielded techniques for generating electromagnetic radiation with intensities as high as 10^{22} W/cm^2 [1]. Experiments show ultrapowerful pulses in underdense plasmas produce hot electrons with energies up to hundreds of MeV [2,3]. As argued in Ref. [4], the effect might be due to ponderomotive acceleration of electrons, following large-angle collisions with ions in strong electromagnetic field. Assuming that the laser dispersion is negligible due to the plasma density being small, the model explains the observed power-law spectra and predicts that the particle maximum energy scales as the third power of the field amplitude. This estimate is also in approximate agreement with the available experimental data [4]; however, the latter is insufficient to conclude whether the model is, in fact, quantitatively accurate. On the other hand, the already small yet nonvanishing densities of the plasma can undermine the assumption of negligible dispersion and therefore modify the acceleration mechanism: the electron velocity can then exceed the group velocity of a laser pulse, so the particles can be reflected, or "snow-plowed" by the field envelope. Thus, to understand the production of hot electrons in previous and future experiments, the effect of the laser dispersion on ponderomotive acceleration must be explored.

Although a general theory of the relativistic ponderomotive force in plasma has been formulated [5], so far, the snow-plow acceleration was studied analytically only in specific regimes when the electron motion is exactly integrable. Particularly, Refs. [6–8] assume equal group and phase velocities of the laser, and Refs. [9–12] suppose circular polarization and *cold* electrons (i.e., having zero transverse momentum), also adopted in Refs. [13–16] for an oscillation-center (OC) model. Hence, the effect of the laser dispersion on the *hot* particle energy gain has not been understood.

The focus of this paper is then twofold. First, we derive the OC Hamiltonian for a relativistic electron injected with an arbitrary momentum in a linearly polarized laser pulse propagating in tenuous plasma, assuming that the pulse length $L_\parallel$ is smaller than the plasma wavelength λ_p. Second, we use this formalism to describe the ponderomotive acceleration of hot electrons generated at collisions with ions under an intense laser drive. Specifically, we identify multiple regimes of this acceleration and show that the laser dispersion affects the process at plasma densities down to $n \sim 10^{17}$ cm^{-3}. We consider the regime when the cold plasma is not accelerated, requiring $a/\gamma_g \ll 1$, where a is the laser parameter, proportional to the field amplitude, and γ_g is the group-velocity Lorentz factor. In this case, the Lorentz factor γ of hot electrons does not exceed $\Gamma \equiv a\gamma_g$ after acceleration, assuming its initial value also satisfies $\gamma_0 \lesssim \Gamma$. Simultaneously, $\gamma \sim \Gamma$ is attained in a wide range of initial conditions, with the angular spread of the accelerated electrons $\chi \sim \gamma_g^{-1}$.

Hence, we conclude that the distribution of hot electrons produced at large-angle collisions with ions at $L_\parallel \ll \lambda_p$ and $a/\gamma_g \ll 1$ must have a cutoff at the energy $\gamma \sim a\gamma_g$. This refines the result from Ref. [4], showing how even weak laser dispersion can affect the acceleration gain. However, further experiments are yet needed to validate the updated scaling because no relevant data has been reported for the regime considered here.

The paper is organized as follows. In Sec. II, we introduce our basic equations. In Sec. III, we derive the OC Hamiltonian for a particle interacting with a laser pulse in tenuous plasma. In Sec. IV, we identify the major regimes of ponderomotive acceleration in plasma and find the general expression for the particle energy gain. In Sec. V, we discuss what we call the plateau regime, where $\gamma \sim \Gamma$ is attained within a wide range of initial conditions. In Sec. VI, we summarize our main results. Supplementary calculations are given in the Appendix.

II. BASIC EQUATIONS

Suppose a plane laser wave propagating in plasma with group velocity v_g and phase velocity v_p along the x axis, so that the vector potential reads as $\mathbf{A} = \mathbf{y}^0 A$,

$$A = \mathcal{A}\left(\frac{x - v_g t}{L_\parallel}\right)\cos(k[x - v_p t]). \tag{1}$$

(We assume no distortion of the pulse due to the plasma dispersion; see Sec. V B.) Here $\mathbf{y}^0$ is a unit vector along the y axis, $L_\parallel$ is the spatial scale of the envelope $\mathcal{A}$, and k is the wavenumber such that $\epsilon \equiv (kL_\parallel)^{-1} \ll 1$. Consider a particle with mass m and charge e interacting with this wave, assuming that the electrostatic potential is negligible (Sec. V B). Then the particle Hamiltonian is [17]

$$\mathrm{H} = c\sqrt{m^2c^2 + p_x^2 + \left(\mathbf{P}_\perp - \frac{e}{c}\mathbf{A}\right)^2}, \tag{2}$$

where p_x is the x component of the particle kinetic momentum, and $\mathbf{P}_\perp = \mathbf{y}^0 P_y + \mathbf{z}^0 P_z$ is the conserved transverse canonical momentum.

In the extended phase space, where $(t, -\mathrm{H})$ serves as another canonical pair and the independent variable is the proper time τ, the equivalent Hamiltonian [18] reads as

$$\mathfrak{H} = \frac{1}{2m}\left[m^2c^2 + p_x^2 + \left(P_y - \frac{e}{c}A\right)^2 + P_z^2 - \frac{\mathrm{H}^2}{c^2}\right], \tag{3}$$

and, numerically, $\mathfrak{H} \equiv 0$. Introduce the dimensionless variables

$$\bar{x} = kx, \quad \rho = p_x/mc, \tag{4a}$$

$$\bar{t} = ckt, \quad \gamma = \mathrm{H}/mc^2, \tag{4b}$$

$$\bar{\tau} = kc\tau, \quad h = \mathfrak{H}/mc^2, \tag{4c}$$

$$\beta_g = v_g/c, \quad \beta_p = v_p/c, \tag{4d}$$

and $\mathtt{P}_{y,z} \equiv P_{y,z}/mc = \text{const}$. Hence, we rewrite Eq. (3) as

$$h = \frac{1}{2}[1 + \rho^2 + (\mathtt{P}_y - \bar{A})^2 + \mathtt{P}_z^2 - \gamma^2], \tag{5}$$

assuming $\bar{\tau}$ is the new time, and the normalized laser field $\bar{A} \equiv eA/mc^2$ reads as

$$\bar{A} = a(\epsilon[\bar{x} - \beta_g \bar{t}])\cos(\bar{x} - \beta_p \bar{t}). \tag{6}$$

III. OSCILLATION-CENTER HAMILTONIAN

A. Extended Hamiltonian

Like in Refs. [6–11,13,14,16], we assume a linear plasma dispersion, which holds for arbitrarily large a at $L_\parallel \ll \lambda_p$ [19–21],

$$\omega^2 = \omega_p^2 + k^2c^2, \tag{7}$$

where $\omega = kv_p$ is the laser frequency, ω_p is the plasma frequency [22]. [Nonlinear instabilities are neglected as they occur on time scales exceeding the acceleration time, which is less than the wave period (Sec. IV B).] Then

$$\beta_g = \sqrt{1 - \alpha}, \quad \beta_p = 1/\sqrt{1 - \alpha}, \quad \alpha = \omega_p^2/\omega^2. \tag{8}$$

Perform a canonical transformation on Eq. (5) [23],

$$(\bar{x}, \rho; \bar{t}, -\gamma) \to (\theta, \mathcal{P}; \psi, \mathcal{W}) \tag{9}$$

governed by the generating function

$$\mathcal{F} = (\bar{x} - \beta_p \bar{t})\mathcal{P} + (\bar{x} - \beta_g \bar{t})\mathcal{W}. \tag{10}$$

Then

$$\rho = \mathcal{P} + \mathcal{W}, \quad \gamma = \beta_p \mathcal{P} + \beta_g \mathcal{W}, \tag{11}$$

so the new Hamiltonian reads as

$$\mathcal{H} = \frac{1}{2}\left\{1 - \frac{\alpha\mathcal{P}^2}{1 - \alpha} + \alpha\mathcal{W}^2 + \mathtt{P}_z^2 + [\mathtt{P}_y - a(\epsilon\psi)\cos\theta]^2\right\}, \tag{12}$$

and the new variables are given by

$$\theta = \bar{x} - \beta_p \bar{t}, \quad \mathcal{P} = \frac{\gamma - \beta_g \rho}{\beta_p - \beta_g}, \tag{13}$$

$$\psi = \bar{x} - \beta_g \bar{t}, \quad \mathcal{W} = -\frac{\gamma - \beta_p \rho}{\beta_p - \beta_g}. \tag{14}$$

Unlike at $\beta_p = \beta_g$ [6–8] (e.g., for vacuum; see the Appendix), or in the exactly integrable case of circular polarization with zero $\mathtt{P}_y$ [9–12], there are two independent coordinates θ and ψ entering $\mathcal{H}$ here; thus, we proceed as follows. Introduce the normalized momenta

$$\overline{\mathcal{P}} = \alpha\mathcal{P}, \quad \overline{\mathcal{W}} = \alpha\mathcal{W}, \tag{15}$$

which remain finite at $\alpha \to 0$; hence, the Hamiltonian

$$\overline{\mathcal{H}} = \frac{1}{2}\left\{\alpha - \frac{\overline{\mathcal{P}}^2}{1 - \alpha} + \overline{\mathcal{W}}^2 + \alpha\mathtt{P}_z^2 + \alpha[\mathtt{P}_y - a(\epsilon\psi)\cos\theta]^2\right\}. \tag{16}$$

Following the general perturbation theory [24–27], we now seek to map out the quiver dynamics. To do this, consider a canonical transformation

$$(\theta, \overline{\mathcal{P}}; \psi, \overline{\mathcal{W}}) \to (\Theta, \hat{\Pi}; \Psi, W) \tag{17}$$

governed by the generating function

$$F = \theta\hat{\Pi} + \psi W + S(\theta, \hat{\Pi}; \psi, W). \tag{18}$$

Choose S such that $\hat{\Pi}$ and W are OC canonical momenta, i.e., the new Hamiltonian $H(\Theta, \hat{\Pi}; \Psi, W)$ does not contain fast oscillations. Then

$$\left\{-\frac{1}{1 - \alpha}[2\hat{\Pi}\partial_\theta S + (\partial_\theta S)^2] + [W\partial_\Psi S + (\partial_\Psi S)^2]^2 + \alpha f(\psi, \theta)\right\}_\sim = 0, \tag{19}$$

the tilde standing for the quiver part, and

$$f(\psi, \theta) = \frac{1}{2}a^2(\epsilon\psi)\cos 2\theta - 2\mathtt{P}_y a(\epsilon\psi)\cos\theta. \tag{20}$$

At $\epsilon \ll 1$, the terms containing $\partial_\psi S$ are negligible; thus, from Eq. (19), S is nearly independent of W, and

$$\Psi = \psi + \partial_W S \approx \psi. \tag{21}$$

Hence, Eq. (19) rewrites as

$$-\frac{1}{1-\alpha}[2\hat{\Pi}\partial_\theta S + (\partial_\theta S)^2 - C^2] + \alpha f(\psi,\theta) = 0, \tag{22}$$

where $C^2 = \langle(\partial_\theta S)^2\rangle$, and the angular brackets denote averaging over θ. Solving Eq. (22) yields

$$S = -\theta\hat{\Pi} + \int^{\theta} \sqrt{\hat{\Pi}^2 + C^2 + \alpha(1-\alpha)f(\psi,\tilde{\theta})}\,d\tilde{\theta}, \tag{23}$$

where we chose the root which corresponds to $\overline{\mathcal{P}} > 0$,

$$\overline{\mathcal{P}} = \hat{\Pi} + \partial_\theta S. \tag{24}$$

Require that S does not contain a zeroth-order harmonic in θ; hence, due to Eqs. (21), (23), and (24), C is found from

$$\int_0^{2\pi} \sqrt{\hat{\Pi}^2 + C^2 + \alpha(1-\alpha)f(\Psi,\tilde{\theta})}\,d\tilde{\theta} = 2\pi\hat{\Pi}. \tag{25}$$

(For an approximate solution see Sec. III C; also see Refs. [13,14,16] for the case $\mathrm{P}_y = \mathrm{P}_z = 0$.) Then, substituting Eqs. (15) and (24) and

$$\overline{\mathcal{W}} = W + \partial_\psi S \approx W \tag{26}$$

into Eq. (16), one gets the new OC Hamiltonian

$$H = \frac{1}{2}\left[\alpha(1 + \mathrm{P}_\perp^2 + 2\Phi) + W^2 - \frac{\hat{\Pi}^2}{1-\alpha}\right], \tag{27}$$

$$\Phi = \frac{a^2}{4}(1-\delta^2), \tag{28}$$

$$\delta^2 = \frac{2C^2}{\alpha(1-\alpha)a^2}, \tag{29}$$

where $\mathrm{P}_\perp^2 \equiv \mathrm{P}_y^2 + \mathrm{P}_z^2$. Hence, we integrate the motion in the variables $(\Theta, \hat{\Pi})$,

$$\hat{\Pi} = \mathrm{const}, \quad \Theta = \hat{\Pi}\overline{\tau}/(1-\alpha) + \mathrm{const}, \tag{30}$$

and the remaining canonical equations read as

$$\dot{W} = -\partial_\Psi H, \quad \dot{\Psi} = W. \tag{31}$$

B. Effective mass M_*

One can also revert to the space and time coordinates, which is done as follows. Apply the variable change

$$\hat{\Pi} = \alpha\bar{\Pi}, \quad W = \alpha\bar{W}, \quad H = \alpha\bar{H}, \tag{32}$$

where $\bar{H}(\Theta, \bar{\Pi}; \Psi, \bar{W})$ is the new Hamiltonian. Perform a canonical transformation

$$(\Theta, \bar{\Pi}; \Psi, \bar{W}) \to (X, \mathrm{P}_x; T, -\mathrm{H}) \tag{33}$$

governed by the generating function

$$\mathrm{F} = \frac{\beta_p\Psi - \beta_g\Theta}{\beta_p - \beta_g}\mathrm{P}_x - \frac{\Psi - \Theta}{\beta_p - \beta_g}\mathrm{H}. \tag{34}$$

Then $\mathrm{P}_x = \langle\rho\rangle$, $\mathrm{H} = \langle\gamma\rangle$, and

$$X = \frac{\beta_p\Psi - \beta_g\Theta}{\beta_p - \beta_g}, \quad T = \frac{\Psi - \Theta}{\beta_p - \beta_g}. \tag{35}$$

Now return from the extended phase space to the physical phase space, so that T becomes the independent variable. Hence, the new Hamiltonian,

$$\mathrm{H} = \sqrt{M_*^2 + \mathrm{P}^2}, \tag{36}$$

is equivalent to that of a particle with an effective mass

$$M_* = \sqrt{1 + 2\Phi}, \tag{37}$$

where $\Phi = \Phi(a, \alpha, \mathrm{P}_y, \Pi)$, where

$$\Pi = \frac{\hat{\Pi}}{\sqrt{1-\alpha}} = \mathrm{H} - \beta_g\mathrm{P}_x \tag{38}$$

is a constant determined by the initial conditions, and $\mathrm{P}^2 = \mathrm{P}_x^2 + \mathrm{P}_\perp^2$ is the OC total momentum squared. Thus, the average force on a particle due to the laser field, or the so-called ponderomotive force, reads as

$$\mathbf{F} = -\langle\gamma\rangle^{-1}\boldsymbol{\nabla} M_*, \tag{39}$$

in the nonrelativistic case yielding $\mathbf{F} \approx -\boldsymbol{\nabla}\Phi$, where Φ is called the ponderomotive potential [28–32].

From Eq. (28), it follows that the electron effective mass and Φ in plasma are less than those in vacuum. As the treatment is expanded to arbitrary dispersion (other polarizations are allowed too), it can also be shown that $M_* < M$ at $\beta_p > 1$, and $M_* > M$ at $\beta_p < 1$ in the general case. However, the sign of the square root in Eq. (23) (and further) must be chosen appropriately, accounting for the fact that $\mathcal{P}$ [Eq. (13)] might then become negative.

C. Explicit approximation for M_*

To find the Hamiltonian H and the effective mass explicitly, solve for δ using Eq. (25), which rewrites as

$$\int_0^{2\pi} \sqrt{\xi^{-2} + \delta^2(\xi, q_y)/2 + \bar{f}(\tilde{\theta}, q_y)}\,d\tilde{\theta} = 2\pi\xi^{-1}, \tag{40}$$

where

$$\xi = a\sqrt{\alpha}/\Pi, \quad q_i = \mathrm{P}_i/a, \quad \bar{f} = f/a^2. \tag{41}$$

At $\xi \ll 1$, $\xi q_y \ll 1$, one can Taylor-expand Eq. (40) and perform the integration; hence, an approximate solution

$$\delta \approx \xi\sqrt{q_y^2 + 1/16}. \tag{42}$$

Then $\delta \ll 1$, so the effective mass reads as

$$M_* = M\left(1 - \frac{a^2\delta^2}{4M^2}\right), \tag{43}$$

where $M = \sqrt{1 + a^2/2}$ is the effective mass in vacuum [16,28,33–37]. Particularly, for cold particles with $\mathrm{P} = 0$ (i.e.,

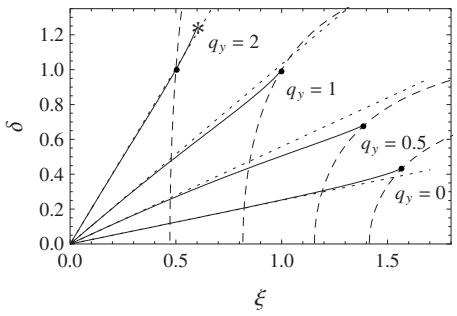

FIG. 1. δ [Eq. (29)] vs $\xi \equiv a\sqrt{\alpha}/\Pi$ for different $q_y \equiv \mathtt{P}_y/a$: dotted: analytical approximation (42); solid: numerical solution of Eq. (25). On the right, each solid line ends at $\xi_*(q_y)$, which is the exact formal upper boundary of the domain, where δ is defined for a given q_y according to Eq. (25). Intersections with $\delta^2(\xi_r, q_\perp)$ [Eq. (46)] (dashed) yield the reflection points ξ_r (bold dots), which satisfy $\xi_r \leq \xi_*$, and physically realizable are $\xi \leq \xi_r$. Here, $\mathtt{P}_z = 0$ and $\alpha \to 0$; thus, $\xi_r \approx \xi_*$ for $q_y = 0, 0.5, 1$, but $\xi_r < \xi_*$ for $q_y = 2$ [in this case, ξ_* is marked with an asterisk $(*)$]. The exact ξ_r is close to those flowing from the analytical approximation, except at $q_y = 0.5$ here. In the latter case, the approximate equation (42) fails to resolve a reflection point (the dashed line *does not* intersect the dotted line); whereas the exact solution shows that the reflection point does exist (the dashed line *does* intersect the dotted line).

$\Pi \approx M$), and $\alpha = \alpha_0/M$ (assuming relativistic modification of the plasma frequency, with $\alpha_0 = \text{const}$), one gets $M_* = M[1 - \alpha_0 a^4/(64M^5)]$, in agreement with Ref. [38].

Equation (42) can also be extrapolated as follows. Equation (40) must hold for any initial conditions; however, at large ξ, its right-hand side goes to zero, and, on the left-hand side ξ^{-2} becomes negligible in comparison with $|\bar{f}| \gtrsim 1$. On the other hand, the square root in Eq. (40) is supposed to remain positive and nonvanishing due to the oscillating $\bar{f}$. Thus, there is no solution for δ at $\xi \gtrsim 1$, meaning that there exists $\xi_*(q_y)$ such that any realizable ξ satisfies

$$\xi \leq \xi_* \lesssim 1 \tag{44}$$

(see also Sec. III D). Yet the exact numerical solution of Eq. (40) for $\delta(\xi, q_y)$ and its domain is close to Eq. (42) for any ξ from the interval $[0, \xi_*(q_y)]$, as seen in Fig. 1. Therefore, Eq. (42) roughly holds for any realizable ξ, and Eq. (37) can be used to—at least—estimate M_* explicitly.

D. Reflection point

Since $\xi \leq \xi_*$, a particle cannot enter a field with $a > a_* \equiv \xi_* \Pi/\sqrt{\alpha}$; thus, if the maximum field exceeds a_*, a particle is reflected. On the other hand, not all ξ satisfying Eq. (44) can be physically realized; thus, a particle may bounce off even a weaker field.

Specifically, the reflection condition is found from

$$\dot{\Psi}^2 + \alpha\left[1 + \mathtt{P}_\perp^2 + \frac{a^2(\epsilon\Psi)}{2}(1 - \delta^2)\right] = \Pi^2, \tag{45}$$

which is obtained using Eq. (27), together with $H \equiv 0$. Suppose $\alpha \ll a^2$; then, at $\dot{\Psi} = 0$, being the condition of particle stopping in the frame traveling with the laser envelope, Eq. (45) yields

$$\delta^2(\xi_r, q_\perp) = 1 + 2(q_\perp^2 - \xi_r^{-2}) \tag{46}$$

for the reflection point ξ_r. Unlike $\xi_*(q_y)$, the value of ξ_r is then determined by both q_y and q_z; hence, $\xi_r < \xi_*$, except at $q_z = 0$ and $|q_y| \leq 1$, for which case one can show $\xi_r \to \xi_*$ for $\alpha \to 0$, as also seen in Fig. 1.

With Eq. (42) used as an estimate for δ [39], one can further show that, in agreement with Refs. [7–11],

$$\xi_r \sim \min\{1, q_\perp^{-1}\}, \tag{47}$$

assuming the inequality (44). Thus, the reflection is impossible at $\xi \ll \xi_r$ and possible at $\xi \sim \xi_r$, whereas larger ξ cannot be realized. Therefore,

$$\xi \leq \xi_r \lesssim 1, \tag{48}$$

which also yields, from Eq. (42) and $q_\perp \geq q_y$, that

$$\delta \lesssim 1. \tag{49}$$

IV. PONDEROMOTIVE ACCELERATION

A. Basic equations

The particle energy γ, as affected by the ponderomotive force (39), can now be calculated as follows. Use Eq. (11) together with Eqs. (15) for $\mathcal{P}$ and $\mathcal{W}$. Further, substitute $\overline{\mathcal{P}}$ from Eq. (24), with S found from Eq. (23), and $\overline{\mathcal{W}}$ from Eq. (26), with $W = \dot{\Psi}$ from Eq. (45); hence,

$$\gamma = \frac{1}{\alpha}\{\sqrt{\Pi^2 + \alpha a^2 \delta^2/2 + \alpha[(a^2/2)\cos 2\theta - 2\mathtt{P}_y a \cos\theta]} \pm \sqrt{(1-\alpha)(\Pi^2 - \alpha[1 + \mathtt{P}_\perp^2 + (a^2/2)(1-\delta^2)])}\}. \tag{50}$$

Thus, the energy retained outside the field is

$$\gamma_\infty = \frac{1}{\alpha}\{\Pi \pm \sqrt{(1-\alpha)(\Pi^2 - \alpha[1 + \mathtt{P}_\perp^2])}\}, \tag{51}$$

where the plus and the minus correspond to the particle overtaking the pulse and falling behind it, respectively.

If no reflection occurs and the average-force approximation [from which Eqs. (50) and (51) are derived] holds on the time interval $(-\infty, +\infty)$ then γ_∞ matches the energy before entering the field, due to the conservation of Π and $\mathtt{P}_\perp$. Yet in the general case,

$$\gamma_\infty \sim \Pi/\alpha, \tag{52}$$

unless $\Pi^2 \gg \alpha(1 + \mathtt{P}_\perp^2)$ and the particle is transmitted. In case of reflection, Eq. (51) can be Taylor expanded in α as

$$\gamma_\infty \approx \frac{1 + \Pi^2 + \mathtt{P}_\perp^2}{2\Pi} \tag{53}$$

[cf. the exact solution (A5) for vacuum].

Hence, γ_∞ can be found by substituting Π from

$$\Pi^2 = w^2 - \alpha a^2[\bar{f} + \delta_0^2/2]. \tag{54}$$

Here, we employed Eqs. (24), (29), (38), and (41) and, using Eqs. (11) and (15), substituted $\overline{\mathcal{P}} = w\sqrt{1-\alpha}$, with

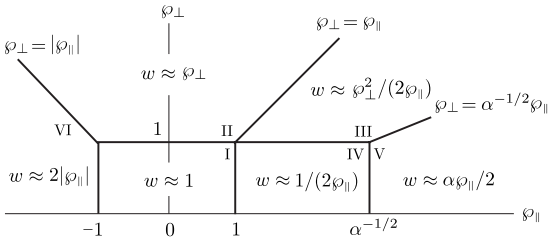

FIG. 2. Scalings for w [Eq. (55)] depending on the normalized initial momentum $\wp$ ($\wp_z=0$, $\alpha\ll 1$). The roman numbers tag distinct regimes.

$$w=\gamma_0-\beta_g\rho_0 \tag{55}$$

found from initial conditions (hence, the index 0). If a particle is born inside the field (Sec. IV B), the initial δ itself depends on Π and must be found from Eqs. (29) and (25) or, approximately, from Eq. (42); yet an estimate can be obtained as follows. From Eqs. (38) and (41), one gets that $\Pi^2/(\alpha a^2)\sim\xi^{-2}\gtrsim 1$, the inequality being due to Eq. (44). Together with Eq. (49), this means that for an estimate, the term proportional to δ^2 can be omitted in Eq. (54), and, since $|f|\sim\max\{1,q_y\}$, one finally gets

$$\Pi^2\sim\max\{w^2,\alpha a^2,\alpha a\mathtt{P}_y\}. \tag{56}$$

B. Regimes of hot-electron acceleration

Consider a hot electron produced inside a laser pulse, e.g., due to ionization or collision (Sec. IV C), at some θ_0 and a on the order of the maximum amplitude $a_{\max}$. Hence, as the particle starts to oscillate, it attains $\gamma\sim\gamma_\infty$ already on a fraction of the oscillation period [Eq. (50)], such as the one described in Ref. [40]. To calculate the associated energy gain, suppose an initial momentum $\wp\equiv\mathbf{p}_0/mc$, for simplicity, assuming $\wp_z=0$ and $\alpha\ll 1$; thus,

$$\mathtt{P}_y=\wp_\perp-a\cos\theta_0\sim\max\{\wp_\perp,a\}, \tag{57}$$

whereas $\wp_\parallel$ will denote the x component of the particle kinetic momentum. Then one of the six regimes is realized, depending on how w [Eq. (55)] is expanded (Fig. 2) and more regimes appear due to Eqs. (56) and (57), allowing multiple scalings for Π and $\mathtt{P}_y$, respectively.

Below, we limit our consideration to only a part of these regimes because of the following. According to Eqs. (47) and (48), a pulse with a maximum amplitude satisfying $\alpha a_{\max}^2\gtrsim 1$ will snow-plow cold electrons of the background plasma, which have $\Pi=1$ and $\mathtt{P}_\perp=0$ [39]. However, this would result in a significant electrostatic potential (ahead of the pulse), which is not included into the model; thus, we assume

$$\alpha a_{\max}^2\ll 1, \tag{58}$$

so only few hot electrons could be snow-plowed. Assuming also $a\gg 1$, twelve distinct regimes persist (Fig. 3) and those of primary interest are discussed below.

C. Acceleration in vacuum

Suppose that an electron is produced at rest, e.g., due to ionization [41,42]; then, from Eq. (57),

$$\mathtt{P}_\perp=a_0\equiv a\cos\theta_0\sim a. \tag{59}$$

At $\alpha\ll 1$, the pulse travels much faster than the particle; hence, the weak dispersion due to plasma is inessential in this case. Then Eq. (54) yields $\Pi\approx w=1$, so $\xi\sim a\sqrt{\alpha}\ll 1$ and $\Pi^2\gg\alpha(1+\mathtt{P}_\perp^2)$, both because of Eq. (58). Therefore, particle reflection from the pulse is impossible in this case (Sec. III D) and Eq. (53) applies, yielding

$$\gamma_\infty=1+a_0^2/2, \tag{60}$$

in agreement with Ref. [40] and regime I in Fig. 3.

When a particle is born with positive $\wp_\parallel\gg 1$, stronger acceleration is predicted from Eq. (53) due to reduced Π. Indeed, suppose a small pitch angle $\chi_0\approx\wp_\perp/\wp_\parallel$ and, again, neglect the plasma dispersion ($\alpha\to 0$); then

$$w\approx\frac{1+\wp_\perp^2}{2\wp_\parallel}\ll 1. \tag{61}$$

Similarly, Eq. (53) holds, so one gets

$$\gamma_\infty\approx\frac{\mathtt{P}_y^2\wp_\parallel}{1+\wp_\perp^2}\sim\frac{a^2\wp_\parallel}{1+\chi_0^2\wp_\parallel^2}, \tag{62}$$

covering regimes III.1 and IV.1 in Fig. 3. Hence, only a small fraction of electrons is accelerated efficiently, particularly, those with $\chi_0\lesssim\wp_\parallel^{-1}\ll 1$. However, the maximum energy now scales as $\gamma_\infty\sim a^2\wp_\parallel$, which is bigger than that flowing from Eq. (60) by the factor $\wp_\parallel\gg 1$.

Note that the effect described here could be anticipated for large-angle electron-ion collisions in tenuous plasmas [4]. Suppose a cold electron oscillating in a laser field with a quiver kinetic momentum $\bar{p}_\sim\sim a$ and zero average velocity. (For the general case, see Fig. 3 and Sec. V.) Suppose further that this particle collides with an ion such that the momentum vector instantaneously rotates toward the pulse propagation direction, i.e.,

$$\wp_\parallel\approx\bar{p}_\sim,\quad \wp_\perp\approx\bar{p}_\sim\chi_0. \tag{63}$$

Then the maximum γ_∞ from Eq. (62) reads as

$$\gamma_\infty\sim a^3, \tag{64}$$

the result being called the a^3-effect [4], and the angular spread of the accelerated electrons is

$$\chi\approx\mathtt{P}_\perp/\gamma_\infty\sim a^{-2}\ll 1. \tag{65}$$

D. Modification of the a^3-effect in plasma

Increasing the number of accelerated electrons requires higher plasma densities, and the a^3-effect is modified in this case because of the laser dispersion; hence, the energy gain is calculated differently. Particularly, for electrons with the initial conditions [Eq. (63)], one has $w\sim a^{-1}$ [Eq. (61); regime IV] and $q_y\sim 1$; then Eq. (56) yields $\Pi^2\sim\max\{\alpha a^2,a^{-2}\}$. At $\sigma\equiv\alpha a_{\max}^4\ll 1$ (regime IV.1), one obtains

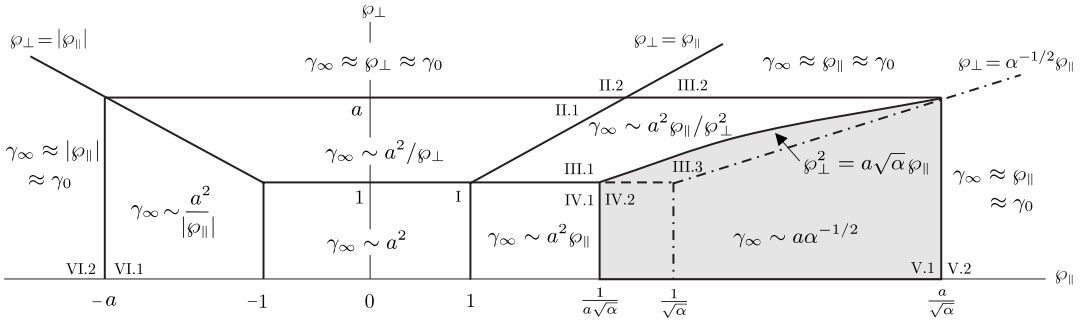

Regime	w [Eq. (55)]	$\mathtt{P}_y$ [Eq. (57)]	Π [Eq. (54)]	γ_∞ [Eq. (51)]
I	$w \approx 1$	$\mathtt{P}_y \sim a$	$\Pi \approx 1$	$\gamma_\infty \sim a^2$
II.1	$w \approx \wp_\perp$	$\mathtt{P}_y \sim a$	$\Pi \approx \wp_\perp$	$\gamma_\infty \sim a^2/\wp_\perp$
II.2	$w \approx \wp_\perp$	$\mathtt{P}_y \approx \wp_\perp$	$\Pi \approx \wp_\perp$	$\gamma_\infty \approx \wp_\perp \approx \gamma_0$
III.1	$w \approx \wp_\perp^2/(2\wp_\parallel)$	$\mathtt{P}_y \sim a$	$\Pi \approx \wp_\perp^2/(2\wp_\parallel)$	$\gamma_\infty \sim a^2\wp_\parallel/\wp_\perp^2$
III.2	$w \approx \wp_\perp^2/(2\wp_\parallel)$	$\mathtt{P}_y \approx \wp_\perp$	$\Pi \approx \wp_\perp^2/(2\wp_\parallel)$	$\gamma_\infty \approx \wp_\parallel \approx \gamma_0$
III.3	$w \approx \wp_\perp^2/(2\wp_\parallel)$	$\mathtt{P}_y \sim a$	$\Pi \sim a\alpha^{1/2}$	$\gamma_\infty \sim a\alpha^{-1/2}$
IV.1	$w \approx 1/(2\wp_\parallel)$	$\mathtt{P}_y \sim a$	$\Pi \approx 1/(2\wp_\parallel)$	$\gamma_\infty \sim a^2\wp_\parallel$
IV.2	$w \approx 1/(2\wp_\parallel)$	$\mathtt{P}_y \sim a$	$\Pi \approx 1/(2\wp_\parallel)$	$\gamma_\infty \sim a\alpha^{-1/2}$
V.1	$w \approx \alpha\wp_\parallel/2$	$\mathtt{P}_y \sim a$	$\Pi \sim a\alpha^{1/2}$	$\gamma_\infty \sim a\alpha^{-1/2}$
V.2	$w \approx \alpha\wp_\parallel/2$	$\mathtt{P}_y \sim \max\{\wp_\perp, a\}$	$\Pi \approx \alpha\wp_\parallel/2$	$\gamma_\infty \approx \wp_\parallel \approx \gamma_0$
VI.1	$w \approx 2\lvert\wp_\parallel\rvert$	$\mathtt{P}_y \sim a$	$\Pi \approx 2\lvert\wp_\parallel\rvert$	$\gamma_\infty \sim a^2/\lvert\wp_\parallel\rvert$
VI.2	$w \approx 2\lvert\wp_\parallel\rvert$	$\mathtt{P}_y \sim \max\{\wp_\perp, a\}$	$\Pi \approx 2\lvert\wp_\parallel\rvert$	$\gamma_\infty \approx \lvert\wp_\parallel\rvert \approx \gamma_0$

FIG. 3. Regimes of ponderomotive acceleration for electrons born inside the laser field with initial momentum $\wp$. The dashed and dot-dashed lines separate formally different domains which correspond to the same maximum energy $\gamma_\infty \sim a\alpha^{-1/2}$, hence, a plateau (shaded), where γ_∞ is independent of $\wp$. The dot-dashed lines are also a *schematic* of the curve (71), at which the particle velocity equals the pulse group velocity. The roman numbers are the same as for the corresponding domains in Fig. 2.

$\Pi \sim a^{-1}$, so the reflection condition is not met, and the plasma effect is negligible. Suppose now that $\sigma \gtrsim 1$ (regime IV.2). Then one gets

$$\Pi \sim a\sqrt{\alpha}, \tag{66}$$

so it becomes possible to reflect electrons from the pulse, at least, for some θ_0. (In vacuum, this effect is impossible because particles could not travel faster than light.) Hence, the final energy is estimated from Eq. (52) as

$$\gamma_\infty \sim a\alpha^{-1/2}, \tag{67}$$

and the angular spread of the accelerated electrons is

$$\chi \approx \mathtt{P}_\perp/\gamma_\infty \sim \sqrt{\alpha} \ll 1. \tag{68}$$

Finally, rewrite Eq. (67) as $\gamma_\infty \sim a^3\sigma^{-1/2}$. Then a uniform scaling is obtained, which covers both regimes IV.1 and IV.2, accounting for how the a^3-effect is modified with the plasma density,

$$\gamma_\infty \sim a^3 \times \min\{1, \sigma^{-1/2}\}. \tag{69}$$

This agrees with the results of our numerical simulations, in which we calculated trial electron orbits using the exact Hamiltonian (16) for a given Gaussian field vector potential using the fourth-order Runge-Kutta method. The particles were introduced at various locations within the laser pulse with the initial condition $\wp = \mathbf{y}^0 a \cos\theta_0$, mimicking electron-ion collisions [cf. Eq. (63)]. The electrons were tracked until they escaped the field, and the final energy γ_∞ was studied as a function of the phase θ_0 and the laser amplitude a at the initial moment. Specifically, at $\sigma \ll 1$ we observed the vacuum a^3-effect, and electron reflection from a pulse was seen at

$$\alpha a_{\max}^4 \gtrsim 4.4. \tag{70}$$

Hence, a sharp dependence of γ_∞ on whether particles are reflected or not [albeit the *scaling* (69) holds for reflected and transmitted electrons equally, as predicted from Eqs. (51) and (52)] and the abrupt elevation in Figs. 4 and 5, both agreeing with Eqs. (67) and (69).

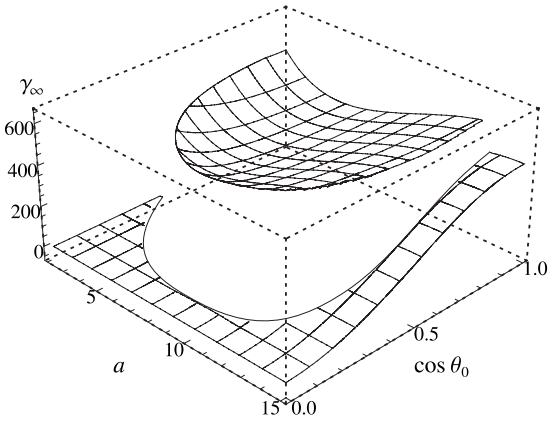

FIG. 4. The final energy $\gamma_\infty = p_x/mc$ of electrons accelerated by a plane laser pulse $a = a_{\max}\exp(-x^2/L_\parallel^2)$ with $L_\parallel = 11\lambda$ in tenuous plasma vs the normalized vector potential envelope $a = e\mathcal{A}/mc^2$ at collision and cosine of the collision phase θ_0; $\alpha = 10^{-3}$, $a_{\max} = 15$, and $\lambda = 2\pi/k$. The elevation corresponds to the electrons being snow-plowed.

V. PLATEAU REGIME

A. Maximum energy gain

Now consider a more realistic case when the electron is also preaccelerated by the pulse *before* the collision; hence, we assume arbitrary initial conditions instead of Eq. (63). Similarly to Sec. IV D, one can show that the acceleration is affected by plasma only in regimes III.3, IV.2, V.I, and V.2 (Fig. 3). Those adjoin the curve

$$\wp_\parallel = \sqrt{\frac{1+\wp_\perp^2}{\alpha}}, \tag{71}$$

which corresponds to the particle traveling at the pulse group velocity, with $\wp_\perp \ll \wp_\parallel$ (dot-dashed in Fig. 3). Hence, the respective interactions are classified as follows.

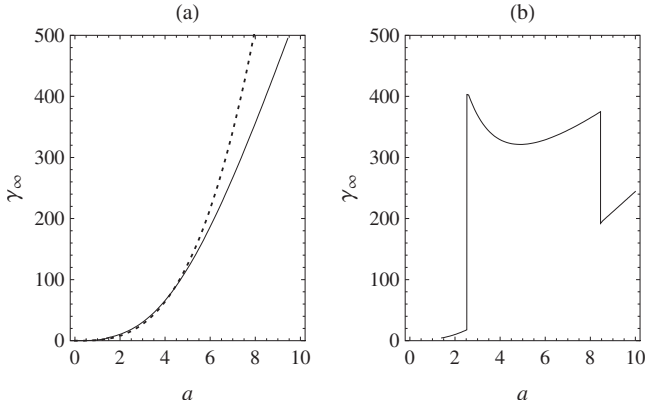

FIG. 5. Same as in Fig. 4 for $\theta_0 = 0$, with $a_{\max} = 10$. (a) $\alpha = 10^{-4}$: numerical (solid) and analytical ($\gamma_\infty = a^3$), corresponding to the a^3-effect (dashed); no particle reflection from the pulse. (b) $\alpha = 10^{-3}$ (numerical); the elevation corresponds to the electrons being snow-plowed.

(i) In regimes III.3 and IV.2, a particle initially travels along x axis slower than the pulse and is accelerated up to the energy (67).

(ii) In regime V.I, a particle initially travels along x axis faster than the pulse. However, it gains additional transverse momentum before it escapes from the field, resulting in the same energy gain (67).

(iii) In regime V.2, a particle is fast enough to run ahead of the pulse such that the energy γ is not affected ($\gamma_\infty \approx \gamma_0$), as opposed to vacuum where $\gamma_\infty \approx \gamma_0 a^2$ would apply at arbitrarily large γ_0 (cf. IV.1).

(iv) In all other regimes, the particle gains energy smaller than both γ_0 and that given by Eq. (67). Thus, for an electron born inside a laser field, one has

$$\gamma_\infty \lesssim \max\{\gamma_0, \Gamma\}, \tag{72}$$

where $\Gamma \equiv a\gamma_g$ is approximately the energy of a particle comoving with the pulse, with the transverse momentum $\bar{p}_\perp \sim a \gg 1$ and the group-velocity Lorentz factor $\gamma_g = \alpha^{-1/2}$.

Assuming $\gamma_0 < \Gamma$, the maximum (over θ_0) of the particle final energy is then attained in the "plateau" formed by the domains III.3, IV.2, and V.I, where it is independent of the initial momentum $\wp$ and so is the angular spread of the accelerated electrons:

$$\gamma_\infty \sim a\gamma_g, \quad \chi \sim \gamma_g^{-1}. \tag{73}$$

Below, we assess the feasibility of the plateau regime and suggest an estimate for the energy of hot electrons, which can be produced in conceivable experiments.

B. Required parameters

The one-dimensional (1D) model above neglects electron escape from the accelerating field in the transverse direction. This is a valid approximation if

$$\Delta\bar{\tau} \lesssim kL_\perp/\bar{p}_\perp, \tag{74}$$

where $\Delta\bar{\tau} \sim \Delta\Psi/\dot{\Psi}$ is the normalized proper time of the interaction, and $\Delta\Psi \sim 1$ because the acceleration occurs on a single period (Sec. IV B). In the plateau regime, Eq. (45) yields $\dot{\Psi} \sim a\sqrt{\alpha}$; thus, Eq. (74) rewrites as

$$L_\perp/\lambda \gtrsim (2\pi\sqrt{\alpha})^{-1}, \tag{75}$$

where we took λ for the laser wavelength, and $\bar{p}_\perp \sim a$. For narrower pulses, the energy gain would be somewhat lower than that predicted by Eq. (73), particularly, for particles born at $\bar{A} \ll a_{\max}$, as also confirmed in our numerical simulations (Fig. 6). Nonetheless, one can anticipate the 1D scaling to hold for feasibly focused ultraintense fields down to about $\alpha \sim 10^{-4}$. Hence, the laser dispersion should affect the electron acceleration at plasma densities down to about 10^{17} cm^{-3}.

Now, let us estimate the influence of the previously neglected wake potential φ, which impedes the acceleration because the associated electrostatic force is directed oppositely to the ponderomotive force [11,43,44]. The energy gain due to the electric field $\mathbf{E}_\varphi = -\boldsymbol{\nabla}\varphi$ is $\gamma_\varphi \sim eE_\varphi L/mc^2$, where $L \sim k^{-1}\Delta\bar{\tau}\gamma_\infty$ is the interaction length, or $kL \sim \gamma_g^2$. As-

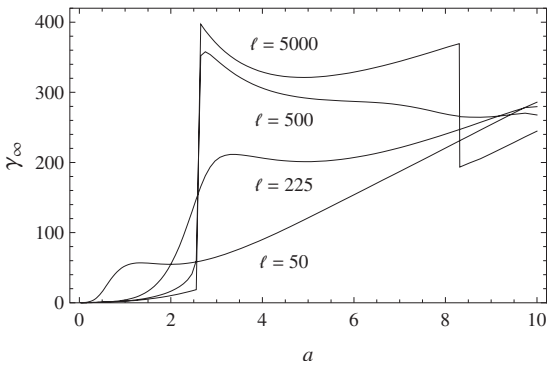

FIG. 6. Same as in Fig. 4 for $\theta_0=0$ and $a_{\max}=10$, but for a *two*-dimensional pulse $a=a_{\max}\exp(-x^2/L_\parallel^2-y^2/L_\perp^2)$ with $L_\parallel=11\lambda$ and different $\ell\equiv L_\perp/\lambda$, where $\lambda=2\pi/k$.

suming the wake spatial scale of about the plasma wavelength $\lambda_p=(k\sqrt{\alpha})^{-1}$ and the density perturbation on the order of n, the Poisson's equation gives $a_\varphi\equiv eE_\varphi/(mc\omega)\sim\sqrt{\alpha}$. Then $\gamma_\varphi\sim a_\varphi kL\sim\alpha^{-1/2}$, yielding $\gamma_\varphi/\gamma_\infty\sim a^{-1}\ll 1$, i.e., the wake is indeed negligible.

For the interaction on the whole pulse length ($L\sim\gamma_g^2 L_\parallel$), one can similarly obtain $\gamma_\varphi/\gamma_\infty\sim L_\parallel/(\lambda a)$. Thus, for ultrashort intense pulses [i.e., such that $L_\parallel/(\lambda a)\ll 1$], φ is, again, insignificant. Similarly, one can show that the laser envelope spreading due to the dilute plasma dispersion can be neglected, as we assumed in Sec. II. Indeed, the pulse spreads significantly only after propagating over a distance $L_s\sim v_g L_\parallel^2(\partial^2\omega/\partial k^2)^{-1}$; with Eq. (7), this gives $L_s\sim kL_\parallel^2/\alpha$ (cf., e.g., Eq. (19) in Ref. [45]). Thus, $L_s/L\sim kL_\parallel\gg 1$, so the approximation of a fixed pulse shape holds on the time scales of our interest.

Hence, Eq. (73) is a valid approximation for estimating the electron final energy. For example, at laser intensity $I\sim 10^{20}$ W/cm^2 and wavelength $\lambda\sim 1$ μm, corresponding to $a\approx[\lambda/(1\ \mu\text{m})][I/(1.37\times 10^{18}\ \text{W/cm}^2)]^{1/2}\sim 10$, and $n\sim 10^{17}$ cm^{-3}, corresponding to $\alpha\sim 10^{-4}$, Eq. (73) predicts $\gamma_\infty\sim 10^3$ and $\chi\sim 0.01$. Therefore, hot electrons can be accelerated to energies of a fraction of GeV and will be scattered within a small angle of 0.6° [46].

VI. CONCLUSIONS

In this paper, we derive the oscillation-center Hamiltonian for an electron injected with an arbitrary momentum in a linearly polarized laser pulse propagating in tenuous plasma, assuming that the pulse length $L_\parallel$ is smaller than the plasma wavelength λ_p. We then use this formalism to describe the ponderomotive acceleration of hot electrons generated at collisions with ions under an intense laser drive. Specifically, we identify multiple regimes of this acceleration and show that the laser dispersion affects the process at plasma densities down to 10^{17} cm^{-3} at intensities 10^{20} W/cm^2. We consider the regime when the cold plasma is not accelerated, requiring $a/\gamma_g\ll 1$, where a is the laser parameter, proportional to the field amplitude, and γ_g is the group-velocity Lorentz factor. In this case, the Lorentz factor γ of hot electrons does not exceed $\Gamma\equiv a\gamma_g$ after acceleration, assuming its initial value also satisfies $\gamma_0\lesssim\Gamma$. Simultaneously, $\gamma\sim\Gamma$ is attained in a wide range of initial conditions, with the angular spread of the accelerated electrons $\chi\sim\gamma_g^{-1}$. Hence, the distribution of hot electrons produced at large-angle collisions with ions at $L_\parallel\ll\lambda_p$ and $a/\gamma_g\ll 1$ will have a cutoff at $\gamma\sim a\gamma_g$. This refines the result from Ref. [4], showing how even weak laser dispersion can affect the acceleration gain. However, further experiments are still needed to validate the updated scaling because no relevant data has been reported for the regime considered here.

ACKNOWLEDGMENTS

This work was supported by the Russian Foundation for Basic Research through Grant No. 08-02-01209-a and the NNSA under the SSAA Program through DOE Research under Grant No. DE-FG52-04NA00139.

APPENDIX: ENERGY GAIN IN VACUUM

In the case of vacuum, a simplified solution is possible as follows. Perform a canonical transformation [23],

$$(\bar{x},\rho;\bar{t},-\gamma)\to(\theta,\rho';\eta,-w), \tag{A1}$$

using a generating function

$$F'=(\bar{x}-\bar{t})\rho'-\bar{t}w. \tag{A2}$$

Then

$$\theta=\bar{x}-\bar{t},\quad \rho'=\rho,\quad \eta=\bar{t},\quad w=\gamma-\rho, \tag{A3}$$

and the transformed extended Hamiltonian is given by

$$h'=1-w^2-2w\rho'+\mathrm{P}_z^2+\{\mathrm{P}_y-a(\epsilon\theta)\cos\theta\}^2\equiv 0.$$

Then w is conserved, yielding an explicit solution for ρ,

$$\rho=\frac{1}{2w}[1-w^2+\mathrm{P}_z^2+\{\mathrm{P}_y-a(\epsilon\theta)\cos\theta\}^2]. \tag{A4}$$

Hence, the particle energy $\gamma=\rho+w$ is obtained, and outside the field one has [cf. Eq. (53)]

$$\gamma_\infty=\frac{1+w^2+\mathrm{P}_\perp^2}{2w}. \tag{A5}$$

[1] G. A. Mourou, T. Tajima, and S. V. Bulanov, Rev. Mod. Phys. **78**, 309 (2006).
[2] S. P. D. Mangles, B. R. Walton, M. Tzoufras, Z. Najmudin, R. J. Clarke, A. E. Dangor, R. G. Evans, S. Fritzler, A. Gopal, C. Hernandez-Gomez, W. B. Mori, W. Rozmus, M. Tatarakis, A. G. R. Thomas, F. S. Tsung, M. S. Wei, and K. Krushelnick, Phys. Rev. Lett. **94**, 245001 (2005).
[3] S.-Y. Chen, M. Krishnan, A. Maksimchuk, R. Wagner, and D. Umstadter, Phys. Plasmas **6**, 4739 (1999).
[4] A. A. Balakin and G. M. Fraiman, Zh. Eksp. Teor. Fiz. **130**, 426 (2006) [J. Exp. Theor. Phys. **103**, 370 (2006)].
[5] B. M. Boghosian, Ph.D. thesis, University of California-Davies, 1987.
[6] M. Eloy, A. Guerreiro, J. T. Mendonça, and R. Bingham, J. Plasma Phys. **73**, 635 (2006).
[7] J. T. Mendonça, L. O. Silva, and R. Bingham, J. Plasma Phys. **73**, 627 (2007).
[8] J. T. Mendonça, Plasma Phys. Controlled Fusion **51**, 024007 (2009).
[9] C. J. McKinstrie and E. A. Startsev, Phys. Rev. E **54**, R1070 (1996).
[10] C. J. McKinstrie and E. A. Startsev, Phys. Rev. E **56**, 2130 (1997).
[11] C. Du and Z. Xu, Phys. Plasmas **7**, 1582 (2000).
[12] E. A. Startsev and C. J. McKinstrie, Phys. Plasmas **10**, 2552 (2003).
[13] N. S. Ginzburg and M. D. Tokman, Fiz. Plazmy **8**, 884 (1982) [Sov. J. Plasma Phys. **8**, 501 (1982)].
[14] N. S. Ginzburg and M. D. Tokman, Zh. Tekh. Fiz. **57**, 409 (1987) [Sov. Phys. Tech. Phys. **32**, 249 (1987)].
[15] J. M. Rax, Phys. Fluids B **4**, 3962 (1992).
[16] M. D. Tokman, Fiz. Plazmy **25**, 160 (1999) [Plasma Phys. Rep. **25**, 140 (1999)].
[17] L. D. Landau and E. M. Lifshitz, *The Classical Theory of Fields* (Pergamon Press, New York, 1971), Sec. 16.
[18] I. Y. Dodin and N. J. Fisch, Phys. Plasmas **13**, 103104 (2006).
[19] C. D. Decker and W. B. Mori, Phys. Rev. E **51**, 1364 (1995).
[20] P. Sprangle, E. Esarey, and A. Ting, Phys. Rev. Lett. **64**, 2011 (1990).
[21] The numerical simulations reported in Ref. [12] confirm that the linear plasma model is reasonably accurate for calculating the electron ponderomotive acceleration by a laser pulse with $a \gg 1$ and $L_{\parallel} \ll \lambda_p$.
[22] The dispersion (8) due to plasma ([46], Sec. 7.9) can also be attributed to a waveguide structure ([46], Sec. 8.3).
[23] The transverse variables remain intact, so the corresponding terms in the generating functions are omitted.
[24] V. I. Arnold, V. V. Kozlov, and A. I. Neishtadt, *Dynamical Systems III* (Springer, New York, 1988).
[25] R. L. Dewar, Phys. Fluids **16**, 1102 (1973).
[26] S. Johnston, A. N. Kaufman, and G. L. Johnston, J. Plasma Phys. **20**, 365 (1978).
[27] S. Johnston and A. N. Kaufman, J. Plasma Phys. **22**, 105 (1979).
[28] I. Y. Dodin and N. J. Fisch, Phys. Rev. E **77**, 036402 (2008).
[29] I. Y. Dodin and N. J. Fisch, Phys. Rev. E **79**, 026407 (2009).
[30] A. V. Gaponov and M. A. Miller, Zh. Eksp. Teor. Fiz. **34**, 242 (1958) [Sov. Phys. JETP **7**, 168 (1958)].
[31] H. Motz and C. J. H. Watson, Adv. Electron. **23**, 153 (1967).
[32] J. R. Cary and A. N. Kaufman, Phys. Rev. Lett. **39**, 402 (1977).
[33] T. W. B. Kibble, Phys. Rev. **150**, 1060 (1966).
[34] D. Bauer, P. Mulser, and W. H. Steeb, Phys. Rev. Lett. **75**, 4622 (1995).
[35] A. Bourdier and S. Gond, Phys. Rev. E **63**, 036609 (2001).
[36] B. Quesnel and P. Mora, Phys. Rev. E **58**, 3719 (1998).
[37] I. Y. Dodin, N. J. Fisch, and G. M. Fraiman, Zh. Eksp. Teor. Fiz. **78**, 238 (2003) [JETP Lett. **78**, 202 (2003)].
[38] J. M. Rax and N. J. Fisch, Phys. Rev. Lett. **69**, 772 (1992).
[39] Equation (42) is not accurate enough to predict the actual reflection point at $q_y \sim 1$ (except at $q_z \gg 1$); e.g., Fig. 1 shows no common solution for Eqs. (42) and (46) at $q_y = 0.5$. On the other hand, at $q_\perp = 0$, the latter equations yield $\xi_r^2 = 4(2-\sqrt{2}) \approx 2.34$, which agrees with the results of our single-particle simulations.
[40] I. Y. Dodin and N. J. Fisch, Phys. Rev. E **68**, 056402 (2003).
[41] S. X. Hu and A. F. Starace, Phys. Rev. Lett. **88**, 245003 (2002).
[42] S. X. Hu and A. F. Starace, Phys. Rev. E **73**, 066502 (2006).
[43] T. Esirkepov, S. V. Bulanov, M. Yamagiwa, and T. Tajima, Phys. Rev. Lett. **96**, 014803 (2006).
[44] G. Shvets, N. J. Fisch, and A. Pukhov, IEEE Trans. Plasma Sci. **28**, 1194 (2000).
[45] E. Esarey and W. P. Leemans, Phys. Rev. E **59**, 1082 (1999).
[46] J. D. Jackson, *Classical Electrodynamics* (Wiley, New York, 1975).